Original article

Marina Cabrini*, Sergio Lorenzi, Simone Pellegrini and Tommaso Pastore

Environmentally assisted cracking and hydrogen diffusion in traditional and high-strength pipeline steels

Abstract: This article deals with the risk of environmentally assisted cracking of steel structures that are kept under cathodic protection (CP). The experimental results collected on both hydrogen diffusion and hydrogen embrittlement (HE) of high-strength low-alloy (HSLA) steels under CP are discussed. Hydrogen diffusion was evaluated by permeation experiments and a scanning photoelectrochemical current technique, as a function of microstructure orientation, on both loaded and unloaded specimens. HE tests were carried out under constant load, slow strain rate (SSR tests), and slow bending conditions. Tests were also carried out on several grades of HSLA steel having different microstructures. The results confirm that HE in artificial seawater under CP can occur in steel with tensile yield strength in the range of 400–660 MPa only in the presence of high cathodic polarization and continuous plastically straining conditions. HE susceptibility increased with increasing applied cathodic polarization and with decreasing strain rate. HE susceptibility of the rolled steels at relatively high strain rate (10^{-4} to 10^{-5} s^{-1}) increased with the hydrogen diffusion coefficient. Similar results were observed in terms of the HE contribution to corrosion fatigue crack growth rate. High-temperature-tempered martensitic steels showed a lower HE susceptibility.

Keywords: cathodic protection; high-strength low-alloy (HSLA) steels; hydrogen diffusion; hydrogen embrittlement; pipeline steels.

*Corresponding author: Marina Cabrini, Department of Engineering and Applied Sciences, University of Bergamo, Italy, e-mail: marina.cabrini@unibg.it
Sergio Lorenzi, Simone Pellegrini and Tommaso Pastore: Department of Engineering and Applied Sciences, University of Bergamo, 24044 Bergamo, Italy

1 Introduction

Buried pipelines and sea lines are normally protected against general corrosion by cathodic protection (CP).

Although the transport of gases and liquids through pipelines is an established and secure technology, several cases of environmentally assisted cracking (EAC) resulting from the effect of hydrogen in the steel have been reported worldwide (Baker & Fessler, 2008; Shipilov & May, 2006).

At room temperature, atomic hydrogen adsorbed on a metal surface can be produced by the electrochemical reduction of water during steel corrosion or by the application of a CP that is lower than the thermodynamic threshold for hydrogen.

Owing to its high solubility in the metal lattice, adsorbed hydrogen can then diffuse inside the metal, with various consequences that are generally called hydrogen damage. In the presence of a susceptible material and an adequate mechanical stress, brittle fracture of the metal can occur due to the occurrence of hydrogen embrittlement (HE) (Hirth, 1980; Srinivasan & Neeraj, 2014; Wallaert, Depover, Pieters, Arafin, & Verbeken, 2014).

Different theories have been proposed to explain the hydrogen-assisted cracking mechanism (Ayas, Deshpande, & Fleck, 2014; Beachem, 1972; Bernstein & Thompson, 1976; Lynch, 2003; Nagumo, 2004; Oriani, 1972; Srinivasan & Neeraj, 2014; Troiano, 1960). Polarizations at too negative potentials can enhance the risks of HE, and it is also well recognized that the HE susceptibility of steels increases with their mechanical properties (Farrell & Quarrell, 1964; Hardie, Charles, & Lopez, 2006; Sandoz, 1972). Meanwhile, there has been a trend toward increasing the relevant mechanical properties of pipeline steels, particularly as the use of high-strength steel pipelines is cost effective, given the increased pressure of the transmitted oil/gas and the decreased wall thickness of the pipe (Demofonti, Cabrini, Marchesani, & Spinelli, 2008). In recent years, API5L X100 grade steel has been developed and installed in recently constructed pipeline

projects in northern Canada and the Japanese subsea (Corbett, Bowen, & Petersen, 2004; Glover et al., 2003; Jin, Liu, & Cheng, 2010).

Recently, the international standards on CP have been altered to introduce critical values of negative potentials that cannot be exceeded in the case where high-strength steels are used.

The ISO 15589-1:2003 standard specifies that the CP potential of high-strength steels (yield strength above 500 MPa) and corrosion-resistant alloys – such as martensitic and duplex stainless steels – shall be determined correctly to avoid the risk of hydrogen formation at the metal surface.

HE risk, either microbiologically produced or due to CP, has also been considered in the ISO 19902:2007 standard in which it is specified that HE susceptibility increases with the yield strength for steel with specified minimum yield strength (SMYS) values in the range of 460–500 MPa. However, field experience has demonstrated that thermomechanically controlled processed steels with SMYS values between 450 and 480 MPa are not susceptible to HE.

In the field, the observation of HE is mainly associated with the presence of hard spots (Carter & Hyatt, 1977), whereas in the absence of microstructural alterations, few cases were observed and only those in buried pipelines that were subject to slow plastic deformations (Punter, Fikkers, & Vanstaen, 1992), mechanical damages, and landslides (Cabrini, Pistone, Sinigaglia, & Tarenzi, 2000). In this regard, there are numerous laboratory studies reported by different authors on HE on pipelines steels (Bosch, Bayle, Magnin, & Longaygue, 2003; Dong, Liu, Li, & Cheng, 2009; Gu, Yu, Luo, & Mao, 1999; Hinton & Procter, 1983; Kasahara, Isowaki, & Adachi, 1981; Payer, Berry, & Boyd, 1976; Punter, Fikkers, & Vanstaen, 1991; Rebak, Xia, Safruddin, & Szklarska-Smialowska, 1996; Shipilov & May, 2006; Trasatti, 2003; Zielinski & Domzalicki, 2003). Nevertheless, some aspects of this phenomenon remain poorly understood.

The DNV Recommended Practice (DNV-RP-B401) also discusses many details relating to the protection potential of high-strength steel and suggests laboratory tests to evaluate the risk of HE that can occur under CP. For instance, constant extension rate testing (SSR) is applicable to compare susceptibility of steels from the same class (i.e. hot rolled), but a comparison between different classes is not suitable. Constant load, four-point bending specimens, and crack tip opening displacement tests are also proposed.
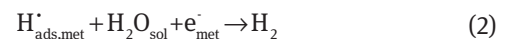
This article summarizes the experimental results collected by the authors on the EAC of high-strength low-alloy

(HSLA) steels under CP to evaluate their HE susceptibility and develop suitable testing methods to compare their respective behavior relative to other steel products.

The results of permeation tests, slow strain rate (SSR) tests, and corrosion-fatigue tests are reported. Finally, the susceptibility of various steels to HE and the corrosion effect on the corrosion-fatigue crack growth are related to the hydrogen diffusion coefficient and tensile strength of the different samples.

2 Cathodic protection and hydrogen evolution

In the absence of hydrogen recombination poisons, such as hydrogen sulfide, the principal factors influencing the HE mechanism in neutral solution are cathodic polarization, intrinsic susceptibility of steel, its metallurgical state, and its loading. The effect of the cathodic polarization derives from the role of the potential (E) on the rate of the cathodic process of hydrogen evolution that mainly occurs, in neutral solutions, from water dissociation according to the reactions:

$$H_2O_{sol} + e^-_{met} \rightarrow H^\cdot_{ads,met} \tag{1}$$

$$H^\cdot_{ads,met} + H_2O_{sol} + e^-_{met} \rightarrow H_2 \tag{2}$$

$$H^\cdot_{ads,met} + H^\cdot_{ads,met} \rightarrow H_2 \tag{3}$$

The entrance of hydrogen into the metal occurs by reaction (1) followed by reaction (4).

$$H^\cdot_{ads,met} \rightarrow H^\cdot_{abs} \tag{4}$$

In neutral water, in contact with oxygen, hydrogen evolution does not occur at the free corrosion potential of steel. However, the CP, which is necessary for the protection against generalized corrosion, shifts the potential below the equilibrium potential for the evolution of hydrogen ($E_{eq,H}$). Generally, CP polarizes the structure at potentials in the range -0.8 to -1.1 V vs. SCE, but overprotection at very negative potentials can be reached, mainly with impressed current systems or with magnesium galvanic anodes, in areas close to the anodes.

The rate of the hydrogen evolution process then increases according to Tafel's law:

$$i_H = i_0 \cdot e^{\frac{E - E_{eq,H}}{B_H}} \tag{5}$$

B_H can be assumed to be equal to about 52 mV at room temperature. In accord with this law, the rate of formation of

atomic hydrogen on a metallic surface under CP increases by one order of magnitude when decreasing the potential (E) by 120 mV.

Nernst's law estimates the equilibrium potential as a function of pH:

$$E_{eq,H} = -59 \cdot pH. \tag{6}$$

At the pH of moist soils, generally from 7 to 8, or seawater, typically 8.2, the equilibrium potential is about -660 to -730 mV vs. SCE. However, the cathodic reaction produces alkalinity on the protected surface, generally in proportion to the cathodic current density. The alkalinization was estimated to increase so as to yield pH 10.5–11 in well-aerated solutions, if calcareous deposit formation does not occur (Cabrini, Lorenzi, Marcassoli, & Pastore, 2011). At such a high pH, the thermodynamic potential for hydrogen evolution on the metal surface falls to the range of -860 to -890 mV vs. SCE.

In natural waters, the pH also increases sufficiently to cause the precipitation of carbonate scale both on marine and buried structures. The formation of calcareous deposits then tends to maintain alkalinity close to the pH of saturation for carbonate precipitation, thus reducing the level of alkalinization. The precipitation of calcium carbonate could lead to an increase of about 100 mV in the potential for hydrogen evolution on the surface of protected structures with respect to those in non-scaling waters, where incrustations do not occur. The effect on the threshold for hydrogen evolution might explain the slight worsening of steel behavior that is observed in artificial seawater with respect to sodium chloride solutions (Cabrini et al., 2011).

3 Hydrogen diffusion

Hydrogen diffusion inside steels has been widely studied using the Devanathan-Stachursky test cell (Devanathan & Stachurski, 1962). Subsequently, modifications were proposed to take into account the effect of the traps and the kinetics of the hydrogen reduction on the cathode surface (Boellinghaus, Hoffmeister, & Dangeleit, 1995; Oriani, 1993; Pressouyre & Bernstein, 1978; Turnbull, Carroll, & Ferriss, 1989; Zakroczymski, 1999, 2006).

The hydrogen flux is proportional to the concentration gradient between the surface and the metal lattice. It depends upon the surface hydrogen concentration, which increases with the hydrogen cathodic overpotential. Additionally, the transport of hydrogen within alloys depends not only on the hydrogen concentration gradient but also on the presence of areas with high hydrostatic stresses (Toribio, 1993; Toribio, Lancha, & Elices, 1991;

Tsay, Chi, Wu, Wu, & Lin, 2006; Yokobori, Nemoto, Satoh, & Yamada, 1996).

According to the theory of Oriani (1970), hydrogen diffusion takes place through the interstitial sites of the crystal structure of metals (normal interstitial lattice sites) or by way of microstructural defects such as dislocations, grain boundaries, interface voids, and atomic impurities that can act as hydrogen traps (Wert, 1978; Wert & Frank, 1983) or preferential paths (Brass & Chanfreau, 1996; Oudriss et al., 2012a,b; Pedersen & Jónsson, 2009; Pressouyre, 1983). Such defects favor diffusion processes owing to their intrinsic low activation energy, but they can also act as potential energy holes that trap hydrogen atoms, thus delaying the penetration into the metal. Traps are usually classified as reversible or irreversible, depending on their binding energy with hydrogen (Fallahmohammadi et al., 2013, 2014a; Hirth, 1980; Kumnick, 1980; Lee & Lee, 1986; Oriani, 1970; Pressouyre, 1983; Pressouyre & Bernstein, 1978; Taha & Sofronis, 2001; Tuyen & Bernstein, 1986; Villalba & Atrens, 2008). Furthermore, saturated reversible traps can behave as sources of hydrogen during transients, hence counteracting reductions of concentration in the lattice (Griffiths & Turnbull, 1995; McNabb & Foster, 1963; Turnbull, Saenz de Santa Maria, & Thomas, 1989).

Generally hydrogen diffusion analysis is based on Fick's second law, although it is not fully applicable in the presence of traps or sources (McNabb & Foster, 1963). The permeation flux through the metal is governed by an apparent diffusion coefficient D_{eff} that can be obtained from experimental measurements.

The diffusion process in pipeline steels is further affected by cold plastic deformations and heat treatments. There is a general agreement as to the effect of cold working on hydrogen permeation. Plastic straining increases the number of dislocations that act as hydrogen traps, increasing hydrogen solubility and resulting in a consequent decrease in D_{eff} (Bockris, Beck, Genshaw, Subramanyan, & Williams, 1971; Bockris, McBreen, & Nanis, 1965; Choo & Lee, 1983; Dietzel, Pfuff, & Juiffs, 2006; Fallahmohammadi et al., 2014a,b; Ha, Ai, & Scully, 2014; Hirth, 1980; Hudson & Straagand, 1960; Kumnick, 1980; Olden, Senumstad Hauge, & Magne Akselsen, 2012; Oriani, 1970; Radhakrishnan & Shreir, 1967; Xie & Hirth, 1982).

4 Effect of strain on hydrogen permeation

The effect of a constant load on the hydrogen permeation flux through a metal membrane has been reported by

several authors (Beck, McBreen, & Nanis, 1966; Blundy, Royce, Poole, & Shreir, 1977; Bockris et al., 1965).

In this work, Figure 1 shows the results of a permeation test performed on ferritic-pearlitic steel polarized at -1.05 V vs. Ag/AgCl in 3% NaCl solution (Cabrini et al., 1995). Two different behaviors for elastic and plastic strain can be seen. The permeation current increases due to strain in the elastic field up to a value of 50% of tensile yield strength (TYS). Following the loading in the plastic field at 100% and 120% TYS, the permeation current steeply increases and then suddenly falls to values lower than the steady-state current. A similar behavior has been observed in steels with acicular ferrite, with bands of bainite and martensite microstructure (Bolzoni, Cabrini, & Spinelli, 2001). The results are in agreement with those of Beck et al. (1966). The permeation current increases due to the enhanced hydrogen solubility in the metal lattice in the elastic field case, whereas the hydrogen diffusion coefficient is not dependent upon the applied stress. Blundy et al. (1977) report a linear correlation between the logarithm of the ratio between the permeation flux in the presence and in absence of stress (J_σ/J_0). This relationship in the elastic field case depends uniquely on the steel microstructure and composition. Bockris and Subramanyan (1971) have ascribed the enhanced solubility of hydrogen in the presence of loading to the decrease in chemical potential in the stressed metal lattice. Taha and Sofronis (2001) have reported that solute hydrogen atoms induce both volume and local modulus changes during straining, and these in turn influence hydrogen penetration in the lattice.

The current peak observed during specimen loading in the plastic field case is due both to the re-passivation of the new surfaces exposed (as demonstrated by tests carried out without hydrogen charging) and to the rapid oxidation of hydrogen, which suddenly occurs at the metal/electrolyte interface. The immediate decrease in the permeation current is due to the trapping effect of the new dislocations generated by the plastic strain. During plastic strain, a large number of dislocations, which act as traps and attract hydrogen atoms from the lattice, are generated and the hydrogen flux consequently decreases. The hydrogen flux reaches a steady-state value once all traps are filled.

Different conditions can arise when hydrogen diffuses within steel under continuous plastic deformation. Dislocations generated by the plastic straining can act either as traps or as preferential pathways (Hirth, 1980; Tien, Nair, & Jensen, 1981; Tien, Thompson, Bernstein, & Richards, 1975). Modifications of the models based on Fick's second law have been proposed by Sofronis and Taha (2000) and Krom and Bakker (2000) to take into consideration the effect of strain rate in the plastic field (Olden et al., 2012; Sofronis, Liang, & Aravas, 2001).

The effect of plastic strain on hydrogen transport in pipeline steels has been experimentally evaluated by hydrogen permeation tests under SSR conditions (Bolzoni et al., 2001; Cabrini, Maffi, & Razzini, 1998). Here the hydrogen permeation current was measured through 1-mm-thick API 5L X60 steel specimens, polarized at -2 V vs. SCE, at different strain rates ranging from 10^{-7} to 10^{-5} s^{-1}. Figure 2 reports the variation in the permeation current (Δi_{perm}) with respect to the steady-state value on unloaded specimens as a function of strain rate. The results were elaborated in order to consider the dependence of passivation current upon the strain rate, which was estimated during SSR tests without any hydrogen charging.

At high strain rates, the filling of new traps results in a depletion of hydrogen concentration in the metal lattice, and a decrease in the permeation flux was observed with
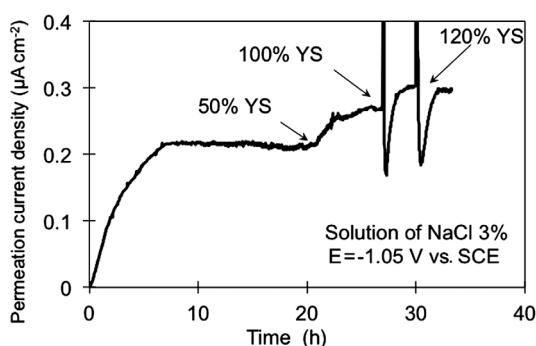

Figure 1: Variation of the hydrogen permeation current through a membrane of API 5L X60 steel under CP at -1.05 V vs. SCE in NaCl solution on the cathodic side after loading at 50%, 100%, and 120% TYS (Cabrini, Razzini, & Tarenzi, 1995).
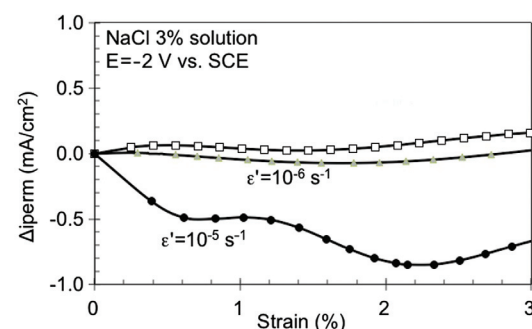

Figure 2: Variation of the permeation current with respect to unloaded specimens (Δi_{perm}) as a function of strain and strain rate (API 5L X60 steel under CP at -2 V vs. SCE on cathodic side of membrane) (Bolzoni et al., 2001).

an increase in the plastic deformation. At strain rates below 10^{-6} s^{-1}, the rate of trap generation is lower than the saturation rate, and hence, depletion cannot occur; the trapping effect becomes negligible with respect to diffusion. Similar results were obtained by several other authors (Bolzoni et al. 2001; Frankel & Latanision, 1986; Hashimoto & Latanision, 1988a,b,c) on X100 steel, polycrystalline nickel, and iron, respectively. Hashimoto and Latanision (1988a,b,c) determined that hydrogen transport by dislocations becomes important when the lattice hydrogen concentration is low and hydrogen is mainly trapped in mobile dislocations.

As the permeation is mainly a monodimensional process, the effect of preferential paths for hydrogen diffusion through steel microstructure cannot be well shown. However, the presence of cracks was noticed during hydrogen permeation tests through X60 steel having a coarse ferritic-pearlitic microstructure. The cracks were found mainly outside the hydrogen-charging window, suggesting that hydrogen diffusion along longitudinal preferential paths is suitable. Cracks were not observed for X100 steel, having a fine-banded microstructure (acicular ferrite and fine pearlite, bainite, and martensite).

5 Effect of microstructure on hydrogen diffusion

Pipelines constructed for carrying natural gas and oil are generally made with HSLA steels. Welded steel pipes with longitudinal seams are manufactured by hot rolling of steel plates, whereas seamless pipes are obtained by piercing mill and hot rolling.

The microstructures of welded pipes are quite different from those of seamless pipes. The former is characterized by ferrite-pearlite microstructures having a grain size dependent upon the rolling temperature and the time intervals between rolling passes. Acicular ferrite and fine pearlite, bainite, and martensite structures can form during hot rolling followed by accelerated cooling processes. A normalization process is generally carried out on seamless pipes producing ferrite and fine pearlite microstructures, but oil quenching and tempering, as alternative heat treatments, gives tempered martensite.

Table 1 reports the hydrogen diffusion coefficients measured in a number of pipeline steels, whereas Table 2 describes their compositions and microstructures. The hydrogen permeation measurements were carried out according to electrochemical methods proposed by Devanathan and Stachurski (1962), and the hydrogen diffusion coefficients were calculated by the application of the time-lag method (Devanathan & Stachurski, 1962; Garet, Brass, Haut, & Guttierez-Solana, 1998; McBreen, Nonis, & Beck, 1966). Many authors have emphasized the role of the method used for the calculation of the hydrogen diffusion coefficient (Turnbull et al., 1989; Zakroczymski, 1999, 2006). The ISO 17081 standard proposes that the evaluation of the hydrogen diffusion coefficient be done using a two-cycle charging/discharging technique to compensate for the contribution of irreversible traps. This method was previously suggested by Turnbull (1994). Fallahmohammadi et al. (2014a,b) and Fallahmohammadi, Bolzoni, Fumagalli, Re, and Lazzari (2013) have recently stated that the hydrogen diffusion coefficient is strictly dependent upon the calculation technique, but they finally concluded that even if the values can be different in terms of magnitude, but they can be considered comparatively.

Table 1: Apparent hydrogen diffusivity (all the values are multiplied by 10^7 cm^2/s) through HSLA steels with different microstructures measured on membranes polarized at -1.05 V vs. SCE on the cathodic side.

Diffusion direction								Steel
			Ferrite-pearlite		Ferrite-bainite	Ferrite-martensite	Tempered martensite	
	X60	X65A	X65B	X65C	X80	X100	X65M	X85M
Rolling (L)	8.5[a]	0.9[b]	2.2[b]	4.4[b]	–	3.9[b]	–	–
		1.9 Pd[b]	2.0 Pd[b]	4.1 Pd[b]				
Short transverse (S)	5.6[a]	2.6[b]	2.2[b]	4.2[b]	4.7[c]	3.9[a]	4.2[c]	4.0[c]
	11.5[c]	2.3 Pd[b]	1.7 Pd[b]	2.4 Pd[b]				
Transverse (T)	–	2.0[b]	1.4[b]	4.6[b]	–	–	–	–
		2.0 Pd[b]	2.0 Pd[b]	3.1 Pd[b]				

[a]Data by Zucchi, Grassi, Frignani, Monticelli, and Trabanelli (2004).
[b]Data by Cabrini, Lorenzi, Marcassoli, & Pastore (2008).
[c]Data by Cabrini, Cogliati, and Maffi (2003) and Cabrini, Migliardi, Pastore, and Spinelli (2003).
Pd specimens with the anodic surface electrochemically covered with palladium.

Table 2: Steel microstructure, mechanical properties, and chemical composition (wt%).

Production process	Steel	$R_{p,0.2}$ (MPa)	R_m (MPa)	C	Mn	Si	P	S	Cr	Ni
Hot rolling	X60[a]	430	588	0.22	1.35	0.24	0.012	0.024	–	0.01
	X65A	399	518	0.09	1.64	0.24	0.003	0.002	0.031	0.017
	X65B	485	567	0.08	1.60	0.31	0.009	0.003	0.053	0.034
Controlled rolling	X65C	507	579	0.05	1.55	0.16	0.002	0.003	0.031	0.005
Controlled rolling-	X80	547	658	0.07	1.89	0.19	0.017	0.006	–	0.28
accelerated cooling	X100[a]	663	750	0.07	1.96	0.34	0.035	0.007	0.03	0.31
Quenched and	X65M	552	619	0.10	1.12	0.30	0.010	0.002	0.142	0.418
tempered	X85M	637[b]	738	0.10	1.11	0.29	0.015	0.002	0.17	0.42

[a]Cabrini et al. (2006).

[b]TYS$_{0.5\%}$.

In this work, the diffusion coefficient was evaluated along the three principal directions: the rolling direction (L), the short transverse direction (S), across thickness, perpendicular to rolling surface, and transverse direction (T), perpendicular to the rolling direction, and short transverse. The measurements were also performed on specimens with palladium electroplating on the anodic detection side of the steel membrane, as suggested by several authors, to obtain meaningful measurements on steel (Manolatos & Jerome, 1996). No significant differences were observed between palladium coated vs. uncoated samples. For banded ferritic-pearlitic steels, some effects due to microstructure could be observed, especially for steels having coarse grain size.

Microstructure strongly influences hydrogen diffusion. In steels with ferritic-pearlitic microstructure, grain boundaries affect the values of the diffusion coefficient. They can either increase the diffusion of hydrogen by providing faster paths for diffusion or reduce the mobility of hydrogen by acting as reversible hydrogen trapping sites at nodes and junction points (Ayesha, Muzaka, Dunne, Calka, & Pereloma, 2013; Choo, Lee, & Cho, 1981; Ichimura, Sasajima, & Imabayashi, 1991; Park, Koh, Jung, & Kim, 2008; Wert, 1978; Yao & Cahoon, 1991; Yazdipour, Haq, Muzaka, & Pereloma, 2012).

Ichitani and Kanno (2003) stated that the main diffusion path in hypo-eutectoid steel are pro-eutectoid ferrite and ferrite. Under non-steady-state charging, hydrogen diffuses along the carbide/ferrite interface because of the trapping effect of the interface.

The microstructural anisotropy of hot-rolled steels strongly influences hydrogen diffusivity. As the pearlite bands act as a barrier against hydrogen diffusion, the hydrogen diffusivity in the banded structure is highly anisotropic. In the random ferrite-pearlite structure, hydrogen can diffuse in all directions, thus its diffusivity is higher than that observed along the transverse and through-surface directions of a banded ferrite-pearlite structure, but lower than that along the longitudinal direction of a banded structure due to preferential diffusion along ferrite bands (Tau & Chan, 1996).

The concentration and orientation of MnS inclusions also affects the diffusivity of hydrogen (Lee & Chan, 1991). Garet et al. (1998) reported that sulfur content has a marked influence on hydrogen permeation and degassing. A lower diffusivity was found for high sulfur content because manganese sulfide acts as trapping site for hydrogen.

Tempered martensitic microstructures are more homogeneous than ferritic-pearlitic microstructures and do not demonstrate anisotropy. The hydrogen diffusivity attains a minimum value in a fresh martensite, whereas diffusivity increases with tempering temperature (Luppo & Ovejero-Garcia, 1991). By contrast, hydrogen solubility decreases with tempering temperature (Fallahmohammadi et al., 2014a,b; Sakamoto, Takao, & Obuchi, 1981). This effect has been attributed predominantly to hydrogen trapping by dislocations, which are defects that are induced by martensite transformation during quenching (Sakamoto et al., 1981).

An interesting discussion of the effect of microstructure on hydrogen diffusion rates was presented by Mindyuk, Svist, Babei, and Karpenko (1971), in which the effect of the carbon in the oversaturated martensite in preventing the diffusion of hydrogen was related to the stress field present in the martensite structure.

6 Hydrogen diffusion visualization through the scanning photo-electrochemical technique

To reveal the effect of texture on hydrogen diffusivity and to show the main diffusion direction, the

photoelectrochemical technique was applied. Razzini, Maffi, Musatti, and Peraldo-Bicelli (1995) have demonstrated that hydrogen permeation through the metal surface alters the photoelectrochemical behavior of steel. In particular, a focused laser beam directed at the anodic side of a steel membrane placed in a modified Devanathan-Starchursky cell with an optical window causes an intensification of the photocurrent, with an increase that is proportional to hydrogen content in the passive film. The effect could conveniently be used to carry out hydrogen mapping through a scanning technique (scanning photoelectrochemical current [SPEC]) (Cogliati, Cabrini, & Maffi, 2003). The photocurrent signal was recorded once a stable passivation condition was reached in the anodic compartment of the cell. The laser beam was synchronized during the scanning to determine the passivation current in the absence of light and the photocurrent in the presence of light. Once the polarization was activated on the cathodic side, the scanning was then repeated to obtain the hydrogen distribution map of diffusion through the steel. Images obtained displayed gray tones ranging from black to white, proportional to photocurrent strength. Cogliati et al. (2003) had applied the SPEC technique on a traditional API 5L X60 steel with a coarse ferrite-pearlite microstructure and also on an experimental X100 steel grade obtained using controlled rolling and accelerated cooling. The specimens were obtained with the rolling bands oriented perpendicularly to the direction of the hydrogen flux. In these measurements, the anodic window was much wider than the cathodic one (0.2 cm^2 for the cathodic and 12.5 cm^2 for the anodic window). The photosignal over the anodic window was recorded to show the variation of hydrogen concentration. Figure 3 shows the photoelectrochemical image of the two specimens after 72 h of charging: the inner circle indicates the cathodic window, whereas the external one corresponds to the anodic one. The dashed lines determine the area in which it was possible to detect the presence of hydrogen.

API 5L X60 steel showed a higher diffusivity rate in the longitudinal direction of hot working than does X100. Diffusion along the banded microstructure reached distances from the central area much greater than the membrane thickness. By contrast, in the X100 steel, the photocurrent signal remains mainly restricted to the center of the anodic area. In this steel, which has a more homogeneous microstructure, the results demonstrate that the flux mainly occurs along the direction of the gradient, through the thickness of the membrane. In addition, the high intensity of the signal in the center of the specimen (white zone) demonstrates the high local concentration of hydrogen in X100 steel compared to the gray uniform color observed in X60 steel.

The photoelectrochemical image of the X60 specimen is larger in the hot rolling direction than in the other direction, demonstrating the preferential distribution of hydrogen along the ferritic-pearlitic bands.

The SPEC technique was also used to demonstrate the hydrogen distribution in an artificial hard spot (Figure 4). A local heat treatment was performed on a 1-mm thickness of API 5L X60 steel using CO_2 laser irradiation (power=100 W, λ=10.6 m) for 30–45 s. Then, martensite was formed locally by water quenching. The metallographic examination confirms the presence of untempered martensite areas inside the artificial hard spot, then a transition zone with martensite, bainite, and fine ferrite-pearlite microstructure between the heat-affected zone and the ferritic-pearlitic base material. A microhardness map is also presented in Figure 4. The photoelectrochemical images demonstrate the higher solubility and lower diffusivity of hydrogen in martensite than in ferrite-pearlite (Razzini et al., 1988).

Hydrogen solubility increases in strained zones at the crack tip, as is shown in Figure 5. The image was
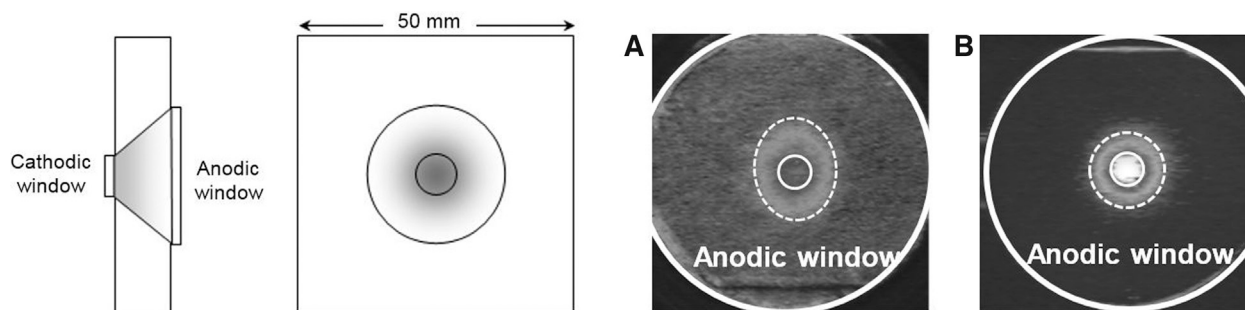

Figure 3: Hydrogen diffusion revealed by photoelectrochemical techniques through (A) API 5L X60 steel and (B) X100 steel (0.2 cm^2 anodic window, 12.5 cm^2 anodic window size) (Cogliati et al., 2003).
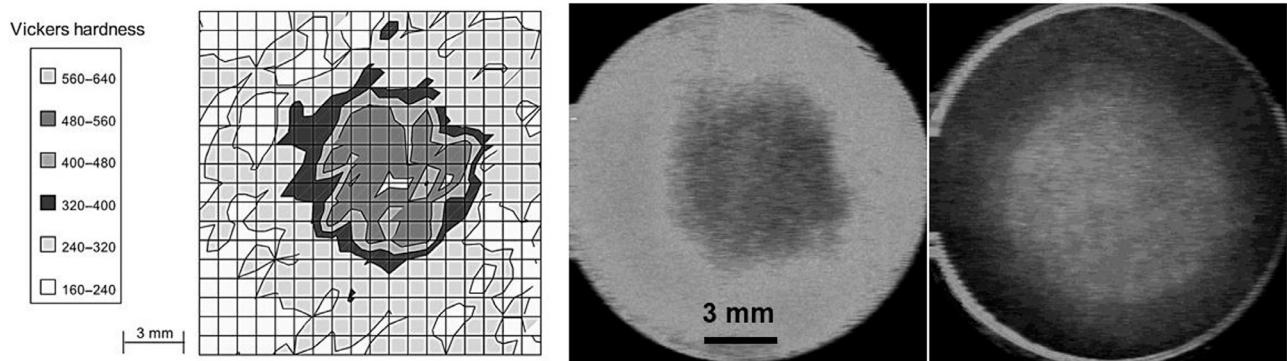
Figure 4: SPEC images of hydrogen diffusion through a low-carbon X60-grade steel containing a hard spot.
(A) Microhardness maps. (B) The martensite structure delays hydrogen diffusion during hydrogen charging. (C) After several hours of hydrogen outgassing, hydrogen remains in martensitic areas (Razzini, Cabrini, Maffi, Musatti, & Peraldo-Bicelli, 1988).

taken on an 80×20×1 mm flat specimen with a 1-mm hole in the center. The specimen was loaded with a sinusoidal waveform at 10 Hz until the initiation of a fatigue crack occurred. Subsequently, the specimen was loaded at 80% of SMYS to produce a wide plasticized region at the crack tips. The loaded specimen was then positioned in a suitable SPEC cell under galvanostatic hydrogen charging (1 mA/cm^2) in borate buffer solution at pH 9 for 4 h. Finally, the specimen was anodically polarized at 0.6 V in NaOH 0.1 M. The photoelectrochemical image was recorded during hydrogen degassing (Razzini et al., 1999).
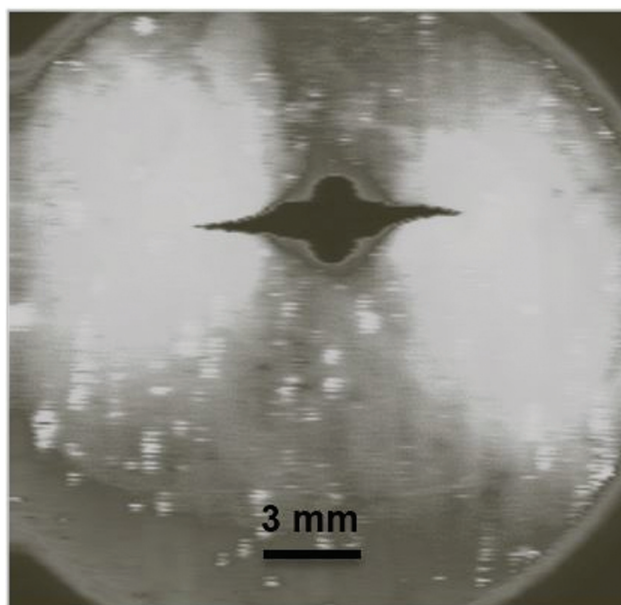

Figure 5: Photoelectrochemical maps of hydrogen concentration in the presence of cracks during constant load tests on precracked specimen (Razzini, Cabrini, Maffi, Mussati, & Peraldo Bicelli, 1999).

7 Hydrogen embrittlement susceptibility of steels

Pipeline steels with strengths ranging from traditional-grade API 5 L X52 (TYS 360 MPa) to more recent X100 (TYS=700 MPa) are substantially immune to HE under constant load conditions and with the usual level of CP, even at very negative cathodic potentials. However, failures were reported due to microstructural modifications, i.e. hard spots (Carter & Hyatt, 1977; Fessler, Groeneveld, & Elsea, 1977), slow plastic deformation (Punter et al., 1992), and mechanical damage and landslides (Cabrini et al., 2000).

An experimental laboratory simulation (Barsanti, Bolzoni, Cabrini, Pastore, & Spinelli, 2007; Bolzoni, Cabrini, Caccia, & Tarenzi, 1993; Cabrini et al., 2008, 2011;) was carried out to determine the critical conditions for onset of HE as a function of potential and strain rate, especially on high-grade steels such as X80 and X100. The latter type is of particular interest due to its possible use for long-distance/high-pressure gas transportation. Results were confirmed by full-scale tests (Demofonti et al., 2008). Failure of specimens has never been observed in such constant load tests, even under overprotection conditions at -1.5 and -2 V vs. SCE. The results demonstrating substantial immunity were also supported by mechanical fracture tests on precracked, modified WOL specimens, which never showed any propagation from fatigue precracking.

During the course of interrupted slow strain rate (ISSR) tests, the specimens also did not show any cracks at -1.05 V vs. SCE. The ISSR tests were carried out using the same experimental apparatus employed for SSR tests. Specimens were initially loaded at a 10^{-5} s^{-1} strain rate. Once maximum load was reached and then a 5% reduction

of load from the maximum value, the elongation was interrupted and the specimen was left in the test solution under constant deformation conditions for 1 week. At the end of this exposure period, the specimen was observed by the scanning electron microscopy (SEM). The presence of microcracks was only observed at -1.5 V vs. SCE on the highest strength grades that were produced by controlled rolling and accelerated cooling.

Only during dynamic SSR tests and slow bending tests performed with continuous slow strain rates in the plastic field was HE observed (Cabrini, D'Urso & Pastore, 2007). Figure 6 shows the typical behavior of SSR curves, whereas Figure 7 shows the fractured surfaces. The higher the cathodic polarization above a critical threshold, the higher the experimental evidence of HE, which produced a loss of ductility in the specimens when compared to reference specimens tested in air. The appearance of HE was also confirmed by SEM observations through the visualization of brittle areas exceeding 50 m depth at different strain rates. Similar results were obtained using slow bending tests (Cabrini et al., 2008) or J-integral tests (Bolzoni, Cabrini, Pedeferri, & Spinelli, 2000).

Figures 8 and 9 (Cabrini et al., 2011) summarize the critical potential for the appearance of HE as a function of strain rate and tensile strength for ferritic-pearlitic steels and martensitic steels, respectively. As expected, HE susceptibility significantly increases at very negative cathodic polarization potentials at the lowest strain rates. Rolled steels showed critical potentials higher than martensitic ones. Steels produced by hot rolling and controlled rolling show similar behavior at the lowest strain rate (1.7×10^{-7} s^{-1}) and potential values approaching that for thermodynamic hydrogen evolution. At higher strain rate, low-strength steels with coarse ferritic-pearlitic microstructures and
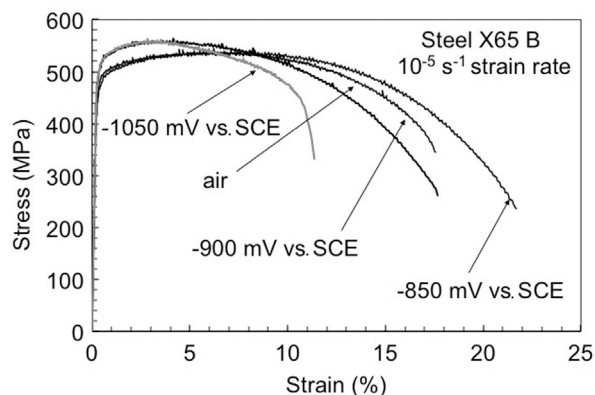

Figure 6: Stress vs. strain curves obtained at 10^{-5} s^{-1} and different potentials for the X65B steel (Cabrini, Lorenzi, Marcassoli, & Pastore, 2006).
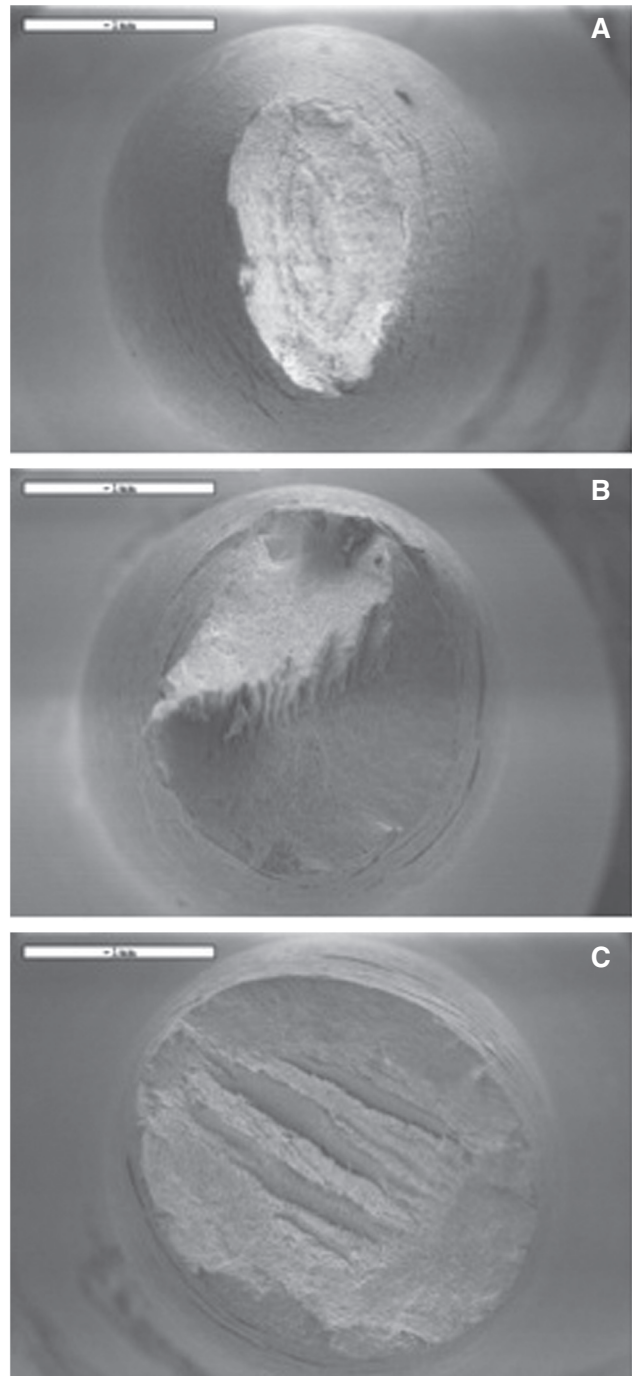

Figure 7: Effect of potential on the fracture surface of the specimens of the X65B steel after the SSR tests (Cabrini et al., 2006). (A) -850 mV vs. SCE. (B) -900 mV vs. SCE. (C) -1050 mV vs. SCE.

high manganese-sulfur content showed higher susceptibility to HE than did high-strength steels.

The mechanical properties of these different steels have been adjusted using slight modifications in the chemical composition and in the parameters regarding
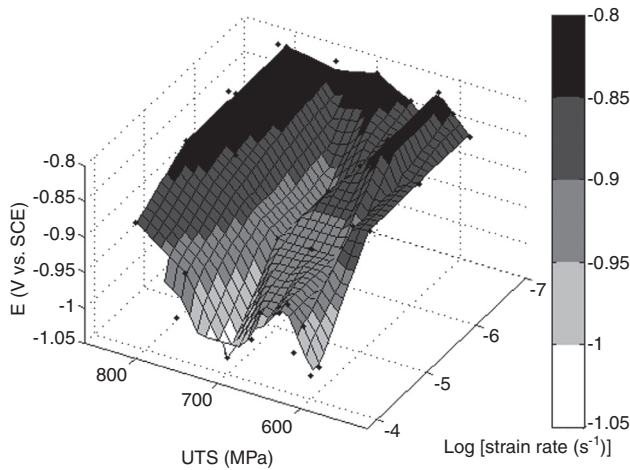
Figure 8: Critical potential for appearance of HE as a function of strain rate and ultimate tensile strength of laminated steels (hot rolling, controlled hot rolling, and controlled hot rolling with accelerated quenching) (Cabrini et al., 2011).
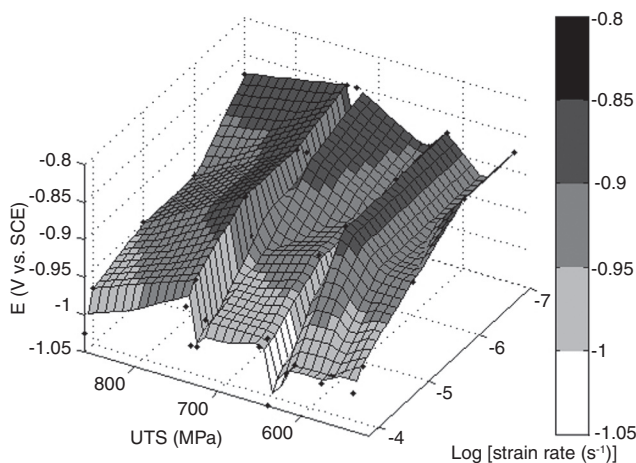

Figure 9: Critical potential for appearance of HE as a function of strain rate and tensile strength of quenched and tempered steels (Cabrini et al., 2011).

consequence, no differences were observed among the various steels considered. By contrast, at high strain rates, i.e. around 10^{-5} s^{-1}, the trapping effect of dislocations strongly influenced the hydrogen permeation within the metal. In this case, a relationship between hydrogen mobility and HE can be observed. Figure 10 shows the relationship between the geometric average of the apparent hydrogen diffusion coefficient in different directions and the HE$_{index}$, obtained by SSR tests at 10^{-5} and -1.05 V vs. SCE polarization. This index defines the susceptibility of the steel to HE and is given in Equation (7):

$$HE_{index} = (1-NRA). \qquad (7)$$

NRA is the normalized reduction of area, which is defined as the ratio between the reduction of area of the specimens after SSR tests in solution and the value measured following the tests in air. A positive correlation can be noted between average hydrogen diffusivity and the effect of HE during SSR test on hot-rolled steels.

When the strain rate is high and the trapping effect prevails over hydrogen supply, hydrogen diffusivity affects embrittlement and the HE effects are more pronounced as hydrogen diffusivity increases. Hot-rolled steels that are characterized by higher diffusivity along the bands allow for a rapid diffusion of hydrogen atoms toward the crack tip, thus favoring the propagation of defects related to environmentally assisted cracking. By contrast, steels having similar hydrogen diffusivity but different microstructures, for example, tempered martensite types, show much lower susceptibility (Figure 10).

Microstructures consisting of spheroidized carbides embedded in a ferritic matrix produced by quenching and tempering rather than a more common normalizing process generally show lower susceptibility to hydrogen cracking in sour environments. It can be hypothesized
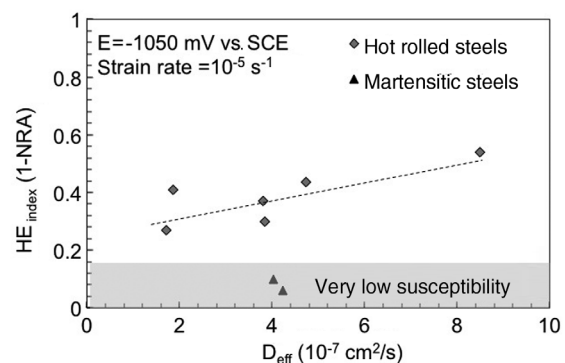
thermomechanical processing. The reduction of the critical potential at low values of UTS is related to the finer pearlite-ferrite microstructures found in rolling and controlled rolling steels, whereas the behavior observed for higher-strength steels is found in the recently developed grades of X80 and X100 having acicular microstructures. In the presence of hard constituents like untempered martensite, the material resistance to HE is significantly decreased (Liao & Lee, 1994; Park et al., 2008).

The permeation measurements carried out under SSRs indicated a negligible effect of the trapping that was created by straining at rates below 10^{-6} s^{-1} because all the dislocations generated are fully saturated. As a

Figure 10: HE index from SSR tests at -1.05 mV vs. SCE as function of the average hydrogen diffusion coefficient (Cabrini et al., 2006).

that they could also behave similarly under CP (Craig & Krauss, 1980; Snape, 1967, 1968; Troiano, 1960).

8 Hydrogen diffusion and corrosion fatigue

HE produced under continuous slow straining can also occur in association with corrosion fatigue produced at low frequencies, over the increasing branch of the loading cycle (Shipilov, 2007). The fatigue behavior of pipeline steels subjected to CP was studied using corrosion fatigue tests performed through single-edged notched-three point bending (Cabrini et al., 2006; Cabrini et al., 2008). The tests were conducted according to the requirements of ASTM E647 standard using sinusoidal loading with minimum to maximum stress ratio (R) equal to 0.6 at 20- and 0.2-Hz frequency used for the tests performed in air and synthetic seawater, respectively. The tests were performed in aerated substitute ocean water (ASTM D1141-75 Standard Specification) under CP at -0.9 and -1.05 V vs. SCE on three ferrite perlite steels (X65A, X65B, and X65C), one ferrite-bainite X80 steel, and two tempered martensitic steels (X65M and X85M). The chemical composition and mechanical properties of the examined steels are given in Table 2.

Figure 11 shows the crack growth rate (da/dN) as a function of the stress intensity factor range (ΔK). The results from test in air show the typical behavior of the Paris' law (Paris & Erdogan, 1963). However, in synthetic seawater under CP, the typical behavior of stress corrosion cracking-corrosion fatigue can be seen. At intermediate values of the stress intensity factor, the crack growth rate reaches a plateau, with an increase compared to the rate measured in air that becomes more pronounced by increasing the cathodic polarization, i.e.
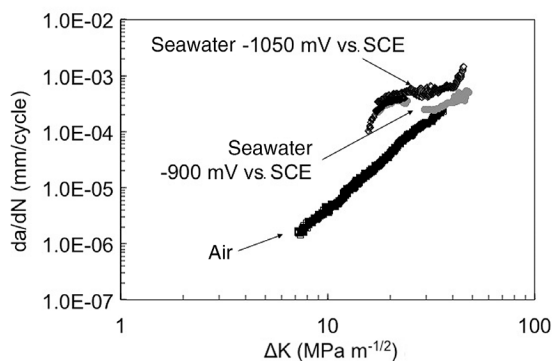
from -0.9 to -1.05 mV vs. SCE potential. At higher stress intensity factors, the curves in air and in synthetic seawater approach each other because the maximum stress intensity factor (K_{Imax}) approaches material fracture toughness. Table 3 shows the threshold values ΔK_{eth} at which the crack growth becomes higher than the corresponding value in air. These values can be related to the K_{ISCC} via the relation shown in Equation (8):

$$K_{ISCC} = \Delta K_{eth} / (1-R). \qquad (8)$$

The corrosion-fatigue crack growth can be analyzed using the model proposed by Wei and Landes (1969). According to their model, the crack growth can be assumed to be the sum of a contribution from pure fatigue, evaluated using the Paris' law $(da/dN)_F$ from air tests, and a contribution from the crack growth from stress corrosion cracking $(da/dN)_C$.

$$\left(\frac{da}{dN}\right)_{C-F} = \left(\frac{da}{dN}\right)_F + \left(\frac{da}{dN}\right)_C \qquad (9)$$

$$\left(\frac{da}{dN}\right)_F = c \cdot \Delta K^n \quad \Delta K_{th} < \Delta K_I < \Delta K_C (1-R) \qquad (10)$$

Figures 12 and 13 show the contribution of stress corrosion cracking to crack growth evaluated by considering Equation (9) and the experimental data in air and under CP at -0.9 mV vs. SCE and -1.05 mV vs. SCE, respectively. The stress corrosion crack growth rate in the plateau zone $(da/dt)_p$ can be estimated using relation (11):

Table 3: Values of ΔK for which the crack growth in the sea environment is higher than the value in air (ΔK_{eth}) and relative to K_{ISCC}.

Steel	Potential (mV vs. SCE)	ΔK_{eth} (MPa·m$^{1/2}$)	K_{Iscc}	ΔK^*
X65A	-900	14	35	23.3
	-1050	13	32.5	21.7
X65B	-900	15	37.5	25
	-1050	14	35	23.3
X65C	-900	17	42.5	28.3
	-1050	15	37.5	25
X65M	-900	–	–	–
	-1050	–	–	–
X80	-900	–	–	–
	-1050	15	37.5	25
X85M	-900	14	35	23.3
	-1050	14	35	23.3

Figure 11: da/dN vs. ΔK curves in air and in artificial seawater at different potentials for X65C steel (Cabrini et al., 2006).

ΔK^* is the value of applied ΔK for which the applied K is always higher than the value of K_{ISCC} ($K_{min} > K_{Iscc}$), $\Delta K^* = K_{Iscc}(1/1-R)$.
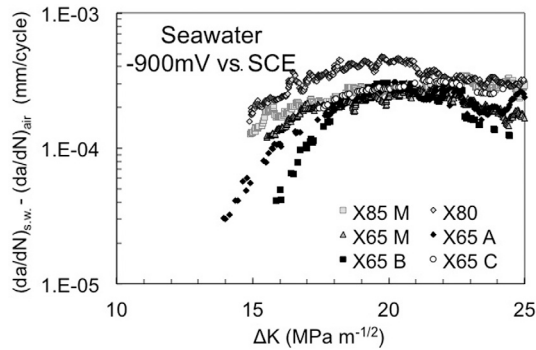
Figure 12: Corrosion contribution to crack growth rate in substitute ocean water at -900 mV vs. SCE (Cabrini et al., 2006).
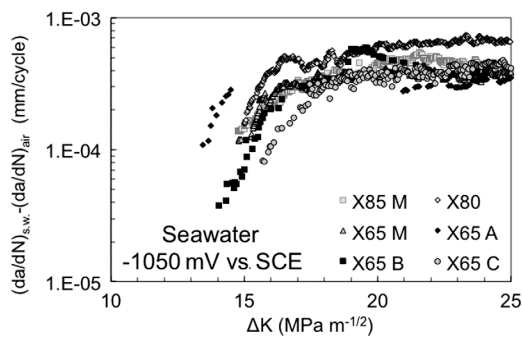

Figure 13: Corrosion contribution to crack growth rate in substitute ocean water at -1050 mV vs. SCE (Cabrini et al., 2006).

$$\left(\frac{da}{dt}\right)_p = \left(\frac{da}{dN}\right)_c \cdot 2 \cdot f, \qquad (11)$$

where f is the load frequency. This relation is valid for K values higher than K_{Iscc} during fatigue cycles. The stress corrosion cracking phenomenon can occur only under tensile conditions at the crack tip, and such a condition is only encountered, to a first approximation, for half the sinusoidal loading cycle. Hence, coefficient 2 was introduced into equation (11). A slight increase in stress corrosion crack growth with higher cathodic polarization can be seen. X80 steel showed the highest propagation rates both at -0.9 and -1.05 V vs. SCE.

At -1.05 V vs. SCE, banded ferrite steels with pearlite, bainite, or martensite structures within the bands showed an increase in the crack propagation rate with the increasing tensile strength of steels. A similar behavior, although less pronounced, was observed for martensitic steels (Figure 14).

Figure 15 relates the plateau crack growth rate due to stress corrosion cracking to the average hydrogen diffusion coefficient. A positive correlation with the diffusivity
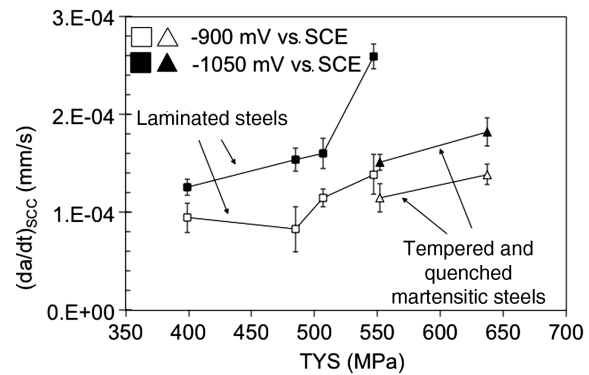

Figure 14: Average crack growth rate in the plateau zone: banded ferritic-pearlitic-bainitic steels and martensitic (Cabrini et al., 2006).
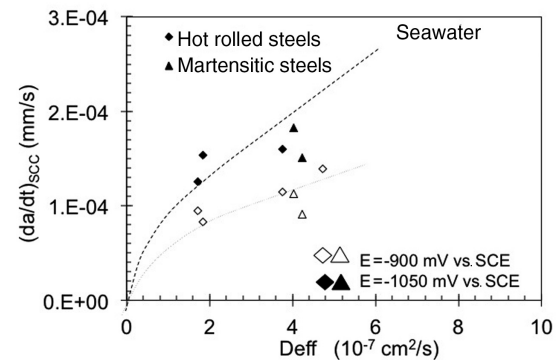

Figure 15: Average crack growth rate evaluated by the Wei and Landes model at -900 and -1050 mV vs. SCE as a function of the average hydrogen diffusion coefficient (Cabrini et al., 2006).

values can be seen as already described for results from SSR tests. In banded ferritic-pearlitic or ferritic-bainitic steels at a potential of -0.9 V vs. SCE, the increase in crack grow rate is quite modest. However, it becomes more pronounced at -1.05 mV vs. SCE.

Just as for the results of SSR tests, steels with a comparable hydrogen diffusion coefficient but with a microstructure of tempered martensite type show lower stress corrosion crack growth. The results confirm the observations of Tau et al. (1993), in which they emphasized the role of a preferred path in banded structures – favoring the hydrogen supply along ferrite-pearlite bands – so as to increase the fatigue crack propagation rate.

9 Conclusions

The article reports and summarizes the experimental results that have been collected by the authors on hydrogen

diffusion rates and the HE of HSLA steels under CP. The experimental results led to the following conclusions:

– Pipeline steels with different microstructures showed different hydrogen diffusivity and HE susceptibility.
– Hot-rolled, controlled hot-rolled, and controlled hot-rolled/accelerated cooled steels characterized by a banded microstructure oriented along the rolling direction showed higher diffusivity than quenched/high-temperature-tempered martensitic steels. The former showed higher values for the hydrogen diffusion coefficient along ferrite-pearlite bands.
– All the steels considered were immune to HE under constant load/strain conditions, but the appearance of the HE phenomenon under SSR conditions could be observed. The HE susceptibility is primarily dependent upon the strain rate and applied potential: hot-rolled steels are more susceptible to HE than quenched and high-temperature-tempered steels.
– Differences between hot-rolled vs. quenched and tempered steels, in terms of their HE susceptibility, can be observed only at high strain rates (10^{-4} to 10^{-5} s^{-1}). At very low strain rates, HE effects are evident for all of the steels at potentials approaching the thermodynamic threshold for hydrogen evolution. A clear positive correlation between the hydrogen diffusion coefficient and HE susceptibility in SSR tests at 10^{-5} s^{-1} strain rate was evident. Higher diffusivity was also found for older steel types that are characterized by high carbon and manganese sulfide inclusion content and by coarse ferrite-pearlite banded microstructure. Modern steels with very fine ferrite-pearlite microstructures showed lower hydrogen diffusion coefficients and, consequently, lower HE susceptibility despite the higher tensile strength. HE susceptibility significantly increases with tensile strength in the presence of untempered martensite areas inside the ferrite bands.
– Similar results were obtained using different specimens and methods, i.e. slow bending tests or J-integral tests as well as corrosion fatigue tests. A correlation between the corrosion contribution to the crack growth rate and the hydrogen diffusion coefficient was determined applying the Wei and Landes model. Results were comparable to those obtained by SSR tests.
– SSR tests at relatively high strain rates (10^{-4} to 10^{-5} s^{-1}) and different cathodic polarization values allow one to evaluate HE susceptibility in steels with similar microstructures. Hence, the behavior of innovative steels can be compared to that of traditional steels for which the susceptibility to HE is well known, as

was suggested by the DNV Recommended Practice guidelines.

References

Ayas C, Deshpande VS, Fleck NA. A fracture criterion for the notch strength of high strength steels in the presence of hydrogen. J Mech Phys Solids 2014; 63: 80–93.

Ayesha JH, Muzaka K, Dunne DP, Calka A, Pereloma EV. Effect of microstructure and composition on hydrogen permeation in X70 pipeline steels. Int J Hydrogen Energy 2013; 38: 2544–2556.

Baker M Jr, Fessler RR. Pipeline corrosion; final report. US Department of Transportation, Pipeline and Hazardous Materials Safety Administration, Office of Pipeline Safety, 2008.

Barsanti L, Bolzoni FM, Cabrini M, Pastore T, Spinelli C. Hydrogen embrittlement resistance of x100 steels for long distance high pressure pipelines. In: Shipilov S, Russell J, Jean-Marc O, Rebak R, editors. Environment-induced cracking of materials – prediction, industrial developments and evaluation. Vol. 1. Oxford, UK: Elsevier, 2007: 291–391.

Beachem CD. A new model for hydrogen-assisted cracking (hydrogen embrittlement). Metall Trans 1972; 3: 437–451.

Beck W, McBreen J, Nanis L. Hydrogen permeation in metals as a function of stress, temperature and dissolved hydrogen concentration. Proc R Soc Lond A 1966; A290: 220–235.

Bernstein M, Thompson AW. Effect of metallurgical variables on environmental fracture. Int Mater Rev 1976; 21: 269–287.

Blundy RF, Royce R, Poole P, Shreir LL. Effect of pressure and stress on permeation of hydrogen through steel. In: Staehle RW, Hochmann J, McCright RD, Slater JE, editors. Stress corrosion cracking and hydrogen embrittlement of iron base alloys. NACE-5. Houston, TX, NACE, 1977: 636–647.

Bockris JO, Subramanyan PK. A thermodynamic analysis of hydrogen in metals in the presence of an applied stress field. Acta Metall 1971; 19: 1205–1208.

Bockris JO, McBreen J, Nanis L. The hydrogen evolution kinetics and hydrogen entry into α-iron. J Electrochem Soc 1965; 112: 1025–1031.

Bockris JO, Beck W, Genshaw MA, Subramanyan PK, Williams FS. The effect of stress on the chemical potential of hydrogen in iron and steel. Acta Metall 1971; 19: 1209–1218.

Boellinghaus TH, Hoffmeister H, Dangeleit A. A scatterband for hydrogen diffusion coefficients in micro-alloyed and low carbon structural steels. Weld World 1995; 35: 83–96.

Bolzoni F, Cabrini M, Caccia M, Tarenzi M. Hydrogen embrittlement of pipelines steels under cathodic protection: comparison of various test methods. In: Costa JM, Mercer AD, editors. Progress in the understanding and prevention of corrosion. Vol. 2. Cambridge, UK: The Institute of Materials, University Press, 1993: 1500–1508.

Bolzoni FM, Cabrini M, Pedeferri P, Spinelli CM. Evaluation of hydrogen embrittlement resistance of micro-alloyed steels by means of J-integral curve. In: Proceedings of Eurocorr 2000, Maney Publishing, London, 2000 (CD).

Bolzoni FM, Cabrini M, Spinelli CM. Hydrogen diffusion and hydrogen embrittlement behaviour of two high strength pipeline steels. In: Proceedings of Eurocorr 2001, Riva del Garda (Bs), AIM Milan, Italy, 2001 (CD).

Bosch C, Bayle B, Magnin T, Longaygue X. Proposal for a critical test to classify the SCC resistance of materials. In: Moody N, Thompson AW, Ricker RE, Was GW, Jones RH, editors. Hydrogen effects on material behavior and corrosion deformation interactions. Warrendale, PA: TMS, 2003: 587–596.

Brass AM, Chanfreau A. Accelerated diffusion of hydrogen along grain boundaries in nickel. Acta Mater 1996; 44: 3823–3831.

Cabrini M, Razzini G, Tarenzi M. Hydrogen permeation and embrittlement of a low alloyed steel. In: Proceedings of NACE International Conference Corrosion in Natural and Industrial Environments: Problems and Solutions, Grado (Gorizia), 1995: 325–333.

Cabrini M, Maffi S, Razzini G. Evaluation of Hydrogen embrittlement behavior by means permeation current measure in slow strain rate conditions of a micro-alloyed steel. In: Bonora P, De Florain F, editors. Electrochemical methods in corrosion research. Materials science forum. Vol. 289–292. Zurich-Uetikon: Transtec Publications, 1998: 1245–1256.

Cabrini M, Pistone V, Sinigaglia E, Tarenzi M. Unique HSC scenario leads to gas line failure. Oil Gas J 2000; 6: 61–65.

Cabrini M, Cogliati O, Maffi S. Effetto della microstruttura sulla diffusione dell'idrogeno in acciai al carbonio per pipeline. Metall Ital 2003; 3: 13–20.

Cabrini M, Migliardi L, Pastore T, Spinelli C. Effect of cathodic potential and strain rate on hydrogen embrittlement of HSLA steels. In: Moody NR, Thompson AW, Ricker RE, Was GW, Jones RH, editors. Hydrogen effects on materials behavior and corrosion deformation interactions. Warrendale, PA: TMS, 2003: 979–988.

Cabrini M, Lorenzi S, Marcassoli P, Pastore T. Hydrogen diffusion and EAC of pipeline steels under cathodic protection. In: Gdoutos EE, editor. Fracture of nano and engineering materials and structures. Proceedings of 16th European Conference of Fracture, Alexandroupolis, Greece: Springer, 2006: 1005–1006.

Cabrini M, D'Urso G, Pastore T. Evaluation of the resistance to hydrogen embrittlement by slow bending test. In: Shipilov S, Russell J, Jean-Marc O, Rebak R, editors. Environment-induced cracking of materials – prediction, industrial developments and evaluation. Vol. 2. Oxford, UK: Elsevier, 2007: 493–502.

Cabrini M, Lorenzi S, Marcassoli P, Pastore T. Effetto della diffusione dell'idrogeno sui fenomeni di EAC di acciai per pipeline in condizioni di protezione catodica. Metall Ital 2008; 100: 15–22.

Cabrini M, Lorenzi S, Marcassoli P, Pastore T. Hydrogen embrittlement behavior of HSLA line pipe steel under cathodic protection. Corros Rev 2011; 29: 261–270.

Carter CS, Hyatt MV. Review of stress corrosion cracking in low alloy steels with yield strength below 150 ksi. In: Staehle RW, Hochmann J, McCright RD, Slater JE, editors. Stress corrosion cracking and hydrogen embrittlement of iron base alloys. NACE-5. Houston, TX: NACE, 1977: 524–600.

Choo WY, Lee JY. Effect of cold working on the hydrogen trapping phenomena in pure iron. Metall Trans A 1983; 14: 1299–1305.

Choo WY, Lee JY, Cho CG. Hydrogen solubility in pure iron and effects of alloying elements on the solubility in the temperature range 20 to 500 C. J Mater Sci 1981; 16: 1285–1292.

Cogliati O, Cabrini M, Maffi S. Effetto della microstruttura sulla diffusione dell'idrogeno in acciai al carbonio per pipeline. Metall Ital 2003; 3: 13–20.

Corbett KT, Bowen RR, Petersen CW. High strength steel pipeline economics. Int J Offshore Polar Eng 2004; 14: 75–79.

Craig BD, Krauss G. The structure of tempered martensite and its susceptibility to hydrogen stress cracking. Metall Trans A 1980; 11A: 1799–1808.

Demofonti G, Cabrini M, Marchesani F, Spinelli CM. Eni TAP project mechanical damage and environmental assisted cracking – full scale methodology overview. In: Proceedings of the International Conference on New Developments on Metallurgy and Applications of High Strength Steels, Buenos Aires, 2008 (CD).

Devanathan MAV, Stachurski Z. The adsorption and diffusion of electrolytic hydrogen in palladium. Proc R Soc Lond A 1962; 270: 90–102.

Dietzel W, Pfuff M, Juiffs GG. Hydrogen permeation in plastically deformed steel membrane. J Mater Sci 2006; 42: 78–84.

Dong CF, Liu ZY, Li XG, Cheng YF. Effects of hydrogen-charging on the susceptibility of X100 pipeline steel to hydrogen-induced cracking. Int J Hydrogen Energ 2009; 34: 9879–9884.

Fallahmohammadi E, Bolzoni FM, Fumagalli G, Re G, Lazzari L. Diffusione e intrappolamento di idrogeno negli acciai per condotte. Metall Ital 2013; 105: 3–13.

Fallahmohammadi E, Bolzoni FM, Fumagalli G, Re G, Ballinger RG, Maruno Y, Lazzari L. Effect of plastic deformation on hydrogen diffusion of X65 pipeline steel. In: Proceedings of NACE Corrosion 2014. Houston, TX: NACE, 2014a. Paper 4390.

Fallahmohammadi E, Bolzoni FM, Fumagalli G, Re G, Benassi G, Lazzari L. Hydrogen diffusion into three metallurgical microstructures of a Ce Mn X65 and low alloy F22 sour service steel pipelines. Int J Hydrogen Energ 2014b; 39: 13300–13313.

Farrell K, Quarrell AG. Hydrogen embrittlement of an ultra-high-tensile steel. Iron Steel Inst Lond 1964; 202: 1002–1011.

Fessler RR, Groeneveld TP, Elsea AR. Stress-corrosion and hydrogen-stress cracking in buried pipelines. In: Staehle RW, Hochmann J, McCright RD, Slater JE, editors. Stress corrosion cracking and hydrogen embrittlement of iron base alloys. NACE-5. Houston, TX: NACE, 1977: 135.

Frankel GS, Latanision RM. Hydrogen transport during deformation in nickel: part I. Polycrystalline nickel. Metall Trans A 1986; 17A: 861–867.

Garet M, Brass AM, Haut C, Guttierez-Solana F. Hydrogen trapping on non metallic inclusions in Cr-Mo low alloy steels. Corros Sci 1998; 40: 1073–1086.

Glover A, Zhou J, Horsley D, Suzuki N, Endo S, Takehara J. Design application and installation of an API5L X100 pipeline. In: Proceedings of the 22nd International Conference on Offshore Mechanics and Arctic Engineering, OMAE2003, Cancun, Mexico, 2003; 37429: 307–318.

Griffiths AJ, Turnbull A. On the effective diffusivity of hydrogen in low alloy steels. Corros Sci 1995; 37: 1879–1881.

Gu B, Yu WZ, Luo JL, Mao X. Transgranular stress corrosion cracking of X-80 and X-52 pipeline steels in dilute aqueous solution with near-neutral pH. Corrosion 1999; 55: 312–318.

Ha HM, Ai JH, Scully JR. Effects of prior cold work on hydrogen trapping and diffusion in API X-70 line pipe steel during electrochemical charging. Corrosion 2014; 70: 166–184.

Hardie D, Charles EA, Lopez AH. Hydrogen embrittlement of high strength pipeline steels. Corros Sci 2006; 48: 4378–4385.

Hashimoto M, Latanision R. Experimental study of hydrogen transport during plastic deformation in iron. Metall Trans A 1988a; 19A: 2789–2798.

Hashimoto M, Latanision R. The role of dislocations during transport of hydrogen in hydrogen embrittlement of iron. Metall Trans A 1988b; 19A: 2799–2803.

Hashimoto M, Latanision R. Theoretical study of hydrogen transport during plastic deformation in iron. Acta Metall 1988c; 36: 1837–1854.

Hinton BRW, Procter RPM. The effect of strain-rate and cathodic potential on the tensile ductility of X-65 pipeline steel. Corros Sci 1983; 23: 101–123.

Hirth JP. Effects of hydrogen on the properties of iron and steel. Metall Trans A 1980; 11A: 861–890.

Hudson RM, Straagand GL. Effect of cold drawing on hydrogen behavior in steel. Corrosion 1960; 16: 253t–258t.

Ichimura M, Sasajima Y, Imabayashi M. Grain boundary effect on diffusion of hydrogen in pure aluminum. Mater Trans JIM 1991; 32: 1109–1114.

Ichitani K, Kanno M. Visualization of hydrogen diffusion in steels by high sensitivity hydrogen microprint technique. Sci Technol Adv Mater 2003; 4: 545–551.

Jin TY, Liu ZY, Cheng YF. Effect of non-metallic inclusions on hydrogen-induced cracking of API5L X100 steel. Int J Hydrogen Energ 2010; 35: 8014–8021.

Kasahara K, Isowaki T, Adachi H. Study on hydrogen-stress cracking susceptibilities of line pipe steels. Vol. 1. Frankfurt/Main: Dechema, 1981.

Krom AHM, Bakker, AD. Hydrogen trapping models in steel. Metall Mater Trans B 2000; 31b: 1475–1482.

Kumnick AJ, Johnson HH. Deep trapping states for hydrogen in deformed iron. Acta Mater 1980; 28: 33–39.

Lee JY, Lee SM. Hydrogen trapping phenomena in metals with B.C.C. and F.C.C. crystals structures by the desorption thermal analysis technique. Surf Coat Technol 1986; 28: 301–314.

Lee HL, Chan SLI. Hydrogen embrittlement of AISI 4130 steel with an alternate ferrite/pearlite banded structure. Mater Sci Eng A 1991; 142: 193–201.

Liao CM, Lee JL. Effect of molybdenum on sulfide stress cracking resistance of low-alloy steels. Corrosion 1994; 50: 695–704.

Luppo MI, Ovejero-Garcia J. The influence of microstructure on the trapping and diffusion of hydrogen in a low carbon steel. Corros Sci 1991; 32: 1125–113.

Lynch SP. Mechanisms of hydrogen assisted cracking – a review. In: Moody NR, Thompson AW, Ricker RE, Was GW, Jones RH, editors. Hydrogen effects on materials behavior and corrosion deformation interactions. Vol. 1. Warrendale, PA: TMS, 2003: 449–466.

Manolatos P, Jerome M. A thin palladium coating on iron for hydrogen permeation studies. Electrochim Acta 1996; 41: 359–365.

McBreen J, Nonis L, Beck W. A method for determination of the permeation rate of hydrogen through metal membranes. J Electrochem Soc 1966; 113: 1218–1222.

McNabb A, Foster PK. A new analysis of the diffusion of hydrogen in iron and ferritic steels. Trans Met Soc AIME 1963; 227: 618–627.

Mindyuk AK, Svist EI, Babei YI, Karpenko GV. Effect of tempering temperature on hydrogen permeability and brittleness of quenched steel (a discussion). Fiz-Khim Mekh Mater 1971; 7: 65–70.

Nagumo M. Hydrogen related failure of steels – a new aspect. Mater Sci Technol 2004; 20: 940–950.

Olden V, Hauge AS, Akselsen OM. The influence of plastic strain on the effective hydrogen diffusion coefficient and trapping in base metal and weld simulated heat affected zone of an X70 pipeline steel. International Society of Offshore and Polar Engineers, 2012.

Oriani RA. The diffusion and trapping of hydrogen in steel. Acta Metall 1970; 18: 147–157.

Oriani RA. Mechanicistic theory of hydrogen embrittlement of steels. Ber Bunsenges Phys Chem 1972; 76: 848–857.

Oriani RA. The physical and metallurgical aspects of hydrogen in metals. In: ICCF-4 Fourth International Conference on Cold Fusion, Lahaina, Maui: Electric Power Research Institute, Palo Alto, CA, 1993. http://lenr-canr.org/acrobat/OrianiRAthephysica.pdf.

Oudriss A, Creus J, Bouhattate J, Conforto E, Berziou C, Savall C, Feaugas X. Grain size and grain-boundary effects on diffusion and trapping of hydrogen in pure nickel. Acta Mater 2012; 60: 6814–6828.

Oudriss A, Creus J, Bouhattate J, Savall C, Peraudeau B, Feaugas X. The diffusion and trapping of hydrogen along the grain boundaries in polycrystalline nickel. Scr Mater 2012; 64: 37–40.

Paris PC, Erdogan F. A critical analysis of crack propagation laws. J Fluids Eng 1963; 85: 528–533.

Park GT, Koh SU, Jung HG, Kim KY. Effect of microstructure on the hydrogen trapping efficiency and hydrogen induced cracking in linepipe steel. Corros Sci 2008; 50: 1865–1871.

Payer JH, Berry WE, Boyd WK. Constant strain rate technique for assessing stress-corrosion susceptibility. Stress corrosion – new approaches. In: ASTM STP 610. Philadelphia, PA: ASTM, 1976: 82–93.

Pedersen A, Jónsson H. Simulations of hydrogen diffusion at grain boundaries in aluminum. Acta Mater 2009; 57: 4036–4045.

Pressouyre GM. Hydrogen traps, repellers, and obstacles in steel. Consequences on hydrogen diffusion, solubility, and embrittlement. Metall Trans A 1983; 14: 2189–2193.

Pressouyre GM, Bernstein IM. Quantitative analysis of hydrogen trapping. Metall Trans A 1978; 9: 1571–1580.

Punter A, Fikkers AT, Vanstaen G. Hydrogen induced stress corrosion cracking of the R.A.P.L. oil transmission pipeline as a result of the combined effect of cathodic protection and plastic deformation. In: Proceedings of the 9th International Pipe Protection Conference, London, 1991: 257–269.

Punter A, Fikkers AT, Vanstaen G. Hydrogen-induced stress corrosion cracking on a pipeline. Mater Perform 1992; 31: 24–28.

Radhakrishnan TP, Shreir LL. Hydrogen permeation through iron and steel by electrochemical transfer – II. Influence of metallurgical factors on hydrogen permeation. Electrochim Acta 1967; 12: 889–903.

Razzini G, Cabrini M, Maffi S, Musatti G, Peraldo-Bicelli L. Effect of the heat-affected zones on hydrogen permeation and embrittlement of low-carbon steels. In: Bonora P, De Florain F, editors. Electrochemical methods in corrosion research materials science forum. Vol. 289–292. Zurich-Uetikon: Transtec Publications, 1988: 1245–1256.

Razzini G, Maffi S, Musatti G, Peraldo-Bicelli L. The scanning photoelectrochemical microscopy of diffusing hydrogen into metals. Corros Sci 1995; 37: 1131–1141.

Razzini G, Cabrini M, Maffi S, Mussati G, Peraldo Bicelli L. Photo-electrochemical visualization in real time of hydrogen distribution in plastic regions of low-carbon steel. Corros Sci 1999; 41: 203–208.

Rebak RB, Xia Z, Safruddin R, Szklarska-Smialowska Z. Effect of solution composition and electrochemical potential on stress corrosion cracking of X-52 pipeline steel. Corrosion 1996; 52: 396–405.

Sakamoto Y, Takao K, Obuchi H. Effects of quenched and tempered microstructures on diffusion of hydrogen in high tensile strength bolt steel. J Soc Mater Sci Jpn 1981; 30: 133–138.

Sandoz G. A unified theory for some effects of hydrogen source, alloying elements, and potential on crack growth in martensitic AISI 4340 steel. Metall Trans 1972; 3: 1169–1176.

Shipilov SA. Solving some key failure analysis problems using advanced methods for materials testing. Eng Failure Anal 2007; 14: 1550–1573.

Shipilov SA, May IL. Structural integrity of aging buried pipelines having cathodic protection. Eng Failure Anal 2006; 13: 1159–1176.

Snape E. Sulfide stress corrosion of some medium and low alloy steels. Corrosion 1967; 23: 154–172.

Snape E. Roles of composition and microstructure in sulfide cracking of steel. Corrosion 1968; 24: 261–282.

Sofronis P, Taha A. Micromechanical modeling of hydrogen transport – a review. In: Kane RD, editor. Environmentally assisted cracking: predictive methods for risk assessment and evaluation of materials, equipment and structures. ASTM STP1401. West Conshohocken, PA: ASTM International, 2000: 70–103.

Sofronis P, Liang Y, Aravas N. Hydrogen induced shear localization of the plastic flow in metals and alloys. Eur J Mech A Solids 2001; 20: 857–872.

Srinivasan R, Neeraj T. Hydrogen embrittlement of ferritic steels: deformation and failure mechanisms and challenges in the oil and gas industry. JOM 2014; 66: 1377–1382.

Taha A, Sofronis P. A micromechanics approach to the study of hydrogen transport and embrittlement. Eng Fract Mech 2001; 68: 803–837.

Tau L, Chan SLI. Effects of ferrite/pearlite alignment on the hydrogen permeation in a AISI 4130 steel. Mater Lett 1996; 29: 143–147.

Tau L, Chan SLI, Shin CS. Effect of anisotropy on hydrogen induced fatigue crack propagation of a banded ferrite/pearlite steel. J Mar Sci Technol 1993; 1: 12–22.

Tien JK, Thompson AW, Bernstein IM, Richards RJ. Hydrogen transport by dislocations. Metall Trans A 1975; 7A: 821–829.

Tien JK, Nair SV, Jensen RR. Dislocation Sweeping of hydrogen and hydrogen embrittlement. In: Bernstein IM, Thompson AW, editors. Hydrogen effects in metals. New York: Metallurgical Society of AIME, 1981: 37–56.

Toribio J. Role of hydrostatic stress in hydrogen diffusion in pearlitic steel. J Mater Sci 1993; 28: 2289–2298.

Toribio J, Lancha AM, Elices M. Macroscopic variables governing the microscopic fracture of pearlitic steels. Mater Sci Eng A 1991; 145: 167–177.

Trasatti SP. Susceptibility on hydrogen embrittlement of an X80 steel for pipelines. In: Moody NR, Thompson AW, Ricker RE, Was GW, Jones RH, editors. Hydrogen effects on materials behavior and corrosion deformation interactions. Vol. 1. Warrendale, PA: TMS, 2003: 959–968.

Troiano AR. The role of hydrogen and other interstitials in the mechanical behaviour of metals. Trans ASM 1960; 52: 54–80.

Tsay LW, Chi MY, Wu YF, Wu JK, Lin DY. Hydrogen embrittlement susceptibility and permeability of two ultra-high strength steels. Corros Sci 2006; 48: 1926–1938.

Turnbull A. Standardization of hydrogen permeation measurement by the electrochemical technique. In: Turnbull A, editor. Hydrogen transport and cracking in metals. London, UK: The Institute of Materials, 1994: 129.

Turnbull A, Carroll MW, Ferriss DH. Analysis of hydrogen diffusion and trapping in a 13% chromium martensitic stainless steel. Acta Metall 1989; 31: 2039–2046.

Turnbull A, Saenz de Santa Maria M, Thomas ND. The effect of H_2S concentration and pH on hydrogen permeation in AISI 410 stainless steel in 5% NaCl. Corros Sci 1989; 29: 89–91, 93–104.

Tuyen DL, Bernstein IM. Hydrogen trapping behavior of spheroidized 1520 steel as a function of plastic strain. Scr Mater 1986; 20: 1025–1029.

Villalba E, Atrens A. SCC of commercial steels exposed to high hydrogen fugacity. Eng Failure Anal 2008; 15: 617–641.

Wallaert E, Depover T, Pieters B, Arafin MA, Verbeken K. TDS evaluation of the hydrogen trapping capacity of NbC precipitates. In: Somerday BP, Sofronis P, editors. International Hydrogen Conference (IHC 2012): Hydrogen-Materials Interactions, 2014. Chapter 62.

Wei RP, Landes JD. Correlation between sustained-load and fatigue crack growth in high strength steel. Mater Res Stand 1969; 9: 43.

Wert CA. Trapping of hydrogen in metals. In: Alefeld C, Volkl J. Hydrogen in metals II. Application-oriented properties. Berlin, Heidelberg: Springer-Verlag, 1978: 305–330.

Wert CA, Frank RC. Trapping of interstitials in metals. Annu Rev Mater Sci 1983; 13: 139–172.

Xie SX, Hirth JP. Permeation of hydrogen, trapping, and damage in spheroidized AISI 1090 Steelpp. Corrosion 1982; 38: 486–493.

Yao J, Cahoon JR. Theoretical modeling of grain boundary diffusion of hydrogen and its effect on permeation curves. Acta Metall Mater 1991; 39: 119–126.

Yazdipour N, Haq AI, Muzaka K, Pereloma EV. 2D modelling of the effect of grain size on hydrogen diffusion in X70 steel. Comput Mater Sci 2012; 56: 49–57.

Yokobori ATJ, Nemoto T, Satoh K, Yamada T. Numerical analysis on hydrogen diffusion and concentration in solid with emission around the crack tip. Eng Fract Mech 1996; 55: 47–60.

Zakroczymski T. Electrochemical determination of hydrogen in metals. J Electroanal Chem 1999; 475: 82–88.

Zakroczymski T. Adaption of the electrochemical permeation technique for studying entry, transport and trapping of hydrogen in metals. Electrochim Acta 2006; 51: 2261–2266.

Zielinski A, Domzalicki P. Hydrogen degradation of high-strength
    low-alloyed steels. J Mater Process Technol 2003; 133:
    230–235.
Zucchi F, Grassi V, Frignani A, Monticelli C, Trabanelli G. Influenza
    degli ioni solfuro sulla permeazione di idrogeno in acciai ad
    alta resistenza. In: Atti convegno nazionale AIM, AIM Milan,
    Vicenza, 2004 (CD).

Bionotes

Marina Cabrini
Department of Engineering and Applied Sciences, University of
Bergamo, Italy
marina.cabrini@unibg.it

Marina Cabrini graduated in Industrial Chemistry from the Uni-
versity of Milan, and is a Professor of Science and Technology of
Materials at the Mechanical Engineering Faculty of the University
of Bergamo since 2001. Her research activity is on electrochemis-
try and corrosion, primary focused on the environmental assisted
cracking of traditional and innovative steels for the oil and gas
industry and light alloys. She is the Italian representative on the
Board of International Corrosion Council.

Sergio Lorenzi
Department of Engineering and Applied Sciences, University of
Bergamo, 24044 Bergamo, Italy

Sergio Lorenzi PhD, graduated in Mechanical Engineering from
the University of Bergamo. He is a researcher at the University of
Bergamo in the Department of Engineering and Applied Science.
He has a PhD in Mechatronic and Applied Technologies, and is an
Adjunct Professor of Science and Technologies of light alloys. His
research activity is on corrosion and protection of metals, tradi-
tional and innovative materials in buildings, cathodic protection.

Simone Pellegrini
Department of Engineering and Applied Sciences, University of
Bergamo, 24044 Bergamo, Italy

Simone Pellegrini is a PhD Student in Engineering and Applied Sci-
ences at the Universityof Bergamo in the Department of Engineering
and Applied Sciences. He has a Master's degree in Building Engi-
neering. He is working on corrosion of rebar in new formulate for
buildings (PhD thesis) and on corrosion and protection of aluminum
alloys produced by means of additive manufacturing.

Tommaso Pastore
Department of Engineering and Applied Sciences, University of
Bergamo, 24044 Bergamo, Italy

Tommaso Pastore has a degree in Nuclear Engineering and a PhD
in Electrochemical Engineering from the Polytechnic of Milan. Since
2001 he is a Full Professor in Corrosion and Protection of Materials
at the University of Bergamo. He was president of the Corrosion
Centre of the Italian Metallurgy Association. His scientific activity is
focused on metallurgy, applied electrochemistry, cathodic protec-
tion, environmentally assisted cracking, corrosion and protection of
materials and durability of reinforced concrete structures.